Progressive worsening of the respiratory and gut microbiome in children during the first two months of COVID-19

Running title: **COVID-19 disturbs children's microbiome**

Rong Xu[1, 4, #], Pengcheng Liu[2, #], Tao Zhang[3, #], Qunfu Wu [3, #], Mei Zeng[2], Yingying Ma[1], Xia Jin[1], Jin Xu[2] *, Zhigang Zhang[3] *, Chiyu Zhang[1, 4] *

1. Shanghai Public Health Clinical Center, Fudan University, Shanghai 201508, China
2. Children's Hospital of Fudan University, Shanghai 201102, China
3. State Key Laboratory for Conservation and Utilization of Bio-Resources in Yunnan, School of Life Sciences, Yunnan University, Kunming, Yunnan 650091, China
4. Pathogen Discovery and Evolution Unit, Institut Pasteur of Shanghai, Chinese Academy of Sciences, Shanghai 200031, China.

# These authors contributed equally to this work.

* Correspondence: Chiyu Zhang, Shanghai Public Health Clinical Center, Fudan University, Shanghai 201508, China. Email zhangcy1999@hotmail.com

Or Zhigang Zhang, State Key Laboratory for Conservation and Utilization of Bio-Resources in Yunnan, School of Life Sciences, Yunnan University, No. 2 North Cuihu Road, Kunming, Yunnan 650091, China. Email: zhangzhigang@ynu.edu.cn.

Or Jin Xu, Department of Clinical Laboratory, Children's Hospital of Fudan University, Shanghai 201102, China. Email: janexu@fudan.edu.cn

Abstract

Children are less susceptible to COVID-19 and manifests lower morbidity and mortality after infection, for which a multitude of mechanisms may be proposed. Whether the normal development of gut-airway microbiome is affected by COVID-19 has not been evaluated. We demonstrate that COVID-19 alters the respiratory and gut microbiome of children. Alteration of the microbiome was divergent between the respiratory tract and gut, albeit the dysbiosis was dominated by genus Pseudomonas and sustained for up to 25-58 days in different individuals. The respiratory microbiome distortion persisted in 7/8 children for at least 19-24 days after discharge from the hospital. The gut microbiota showed early dysbiosis towards later restoration in some children, but not others. Disturbed development of both gut and respiratory microbiomes, and prolonged respiratory dysbiosis in children imply possible long-term complications after clinical recovery from COVID-19, such as predisposition to an increased health risk in the post-COVID-19 era.

Key words: SARS-CoV-2/COVID-19; respiratory microbiota; gut microbiota, dysbiosis; children.

Introduction

COVID-19 caused by SARS-CoV-2 has impacted millions of peoples in more than 200 countries around the world[1,2]. Compared with adults, children appear to be less susceptible to COVID-19 with extremely low morbidity and mortality[3-5]; and children with COVID-19 often have mild symptoms with a faster recovery, and better prognosis. The reasons for these are not entirely clear. Early-life development and maturation of human microbiomes shape health status in later life[6-9], and delayed development or dysbiosis of the microbiomes during childhood has been linked to predisposition to various diseases in adulthood[7-12]. The effect of COVID-19 on the gut microbiome had just began to be evaluated in adults[13,14], but never in children. We recently evaluated the longitudinal effects of COVID-19 on both the respiratory and gut microbiome in adults, and revealed that the respiratory and gut microbiome presented a contemporaneous change from early dysbiosis towards late incomplete restoration during the course of disease (Xu et al., unpublished observation). How COVID-19 impacts on the respiratory and gut microbiomes of children is not known. Here, we report temporal dynamics of respiratory and gut microbiome in children with COVID-19.

Results

Study cohort

Nine COVID-19 children between 7-139 months old were enrolled in this study together with 14 age-matched healthy control children. A total of 103 specimens including 27 sets of paired specimens (at least two of throat swab, nasal swab and feces) were collected from children with COVID-19 (Supplementary Fig. 1). The children were being followed between 25-58 days after symptom onset. All samples were subjected to high-throughput sequencing of the V4-region of bacterial 16S rRNA gene (Methods).

Respiratory and gut microbiome dynamics in COVID-19

We analyzed the 16S-rRNA gene sequences of all specimens from three body sites, and obtained 2,187 sub-OTUs (sOTUs) that represent 15 known phyla including 200 known genera (Supplementary Table 1). Using the DMM method (Supplementary method), we identified 8 community types (Fig.1a). The specimens from healthy children clustered into two community types, one bears the signature of stool samples (H-GUT), and another represents the collection of all three kinds of samples (throat swab, nasal swab and feces) (H-MIX). H-GUT is significantly separated from H-MIX (Fig. 1b), with significantly lower richness and evenness (Fig.1c). H-GUT was featured by *Moraxella*, a commensal in nasal passages of infants, implying that it might not represent a normal gut microbiome status. Because the development of infant microbiome is influenced by maternal materials from multiple sites (stool, vaginal, oral and skin) among which bacteria from maternal gut being the most important contributor[15], infants and children may share the same or very similar microbial community structures of the nasal cavity, throat and gut[16,17]. Therefore, H-MIX represents

the gut and respiratory tract microbiomes of healthy children. In fact, the nasal cavity, throat and gut still maintain similar microbial structures in adulthood.

Bacteria from stool specimens of COVID-19 children fell into three distinct community types (COVID-GUT I-III), and those from nasal and throat swabs formed another three distinct types (COVID-TN I-III) (Fig. 1a). All COVID-19-related types are significantly separated from the type H-MIX except COVID-TN-I that overlaps with H-MIX (Fig. 1b). In particular, three respiratory tract-related types and three GUT-related types of COVID-19 children are also significantly separated from each other, and distinctly different from healthy children. These results indicated that SARS-CoV-2 infection significantly changed the gut and respiratory tract microbiota of children, and the separation of bacterial community structures between the gut and respiratory tracts suggested that the normal development of the microbiota may be impaired.

All COVID-19-related types showed lower richness and evenness than H-MIX, except for COVID-GUT-I that has the most similarity to H-MIX and relatively normal microbiome structure. There was a gradual decrease from community type I to III for both gut and respiratory tract (Fig. 1c), indicating a progressive deterioration (dysbiosis) of the microbiome. Overall, the dysbiosis appeared to be more severe in the respiratory tract than in the gut.

Indicator genera of eight DMM clusters

To characterize eight microbial community types, we identified 35 indicator genera (Fig. 2a). The H-MIX type was characterized by 11 genera, and the predominant commensal bacteria contained *Prevotella, Streptococcus,* unclassified *Pasteurellaceae,* and *Actinomyces* (Fig. 2b). Some of the indicator bacteria in H-MIX were shared by the community types COVID-GUT-I (e.g. *Prevotella,*

Porphyromonas, Finegoldia, Anaerococcus, etc.) and COVID-TN-I (e.g. *Prevotella, Neisseria, Fusobacterium,* unclassified *Pasteurellaceae, Leptotrichia* etc.). As a dysbiosis status, community type COVID-GUT-III was dominated by *Bacteroides,* as well as *Parasutterella* that is associated with irritable bowel syndrome and other intestinal chronic inflammation[18]. Community type COVID-TN-III was dominated by highly abundant *Pseudomonas* and *Herbaspirillum*, and it had higher levels of genera of *Corynebacterium, Comamonadaceae, Burkholderia, Achromobacter, Brevundimonas, Ralstonia, Phyllobacterium,* and *Burkholderiales* than other community types (Fig. 2b). Genus *Pseudomonas* is a notorious human pathogen associated with various diseases (e.g. pneumonia), and the samples were overwhelmed by the dominant species *Pseudomonas veronii* (100% sequence identity)[19]. Apart from COVID-TN-III, genus *Pseudomonas* also dominated community type COVID-TN-II with *Streptococcus*, and COVID-GUT-II with *Bacteroides*. Furthermore, *Achromobacter* and *Burkholderia* are associated with cystic fibrosis[20,21], and most other genera are environmental bacteria. The predominance of *Pseudomonas* together with the colonization of various environmental bacteria in type COVID-TN-III imply an extreme dysbiosis in upper respiratory tract.

The dynamic change of children during COVID-19

Recently, we observed synchronous restoration of the microbiomes of both respiratory tract and the gut towards normal structure in COVID-19 adults within a short time (6-17 days) after symptom onset (Xu et al., unpublished observation). Distinct from adults, the microbiome community compositions were extremely dynamic in children during COVID-19, and the changes of the community types in the respiratory tract and gut were divergent (Fig. 3a). The respiratory (especially nasopharyngeal) microbiome of 7/8 children (except CV05) appeared to evolve from early healthy

(H-MIX) or high-diversity community structures (COVID-TN-I) to late low-diversity dysbiosis structure (COVID-TN-III), indicating a steady deterioration in composition and function of the respiratory microbiome despite a fast clinical recovery (Fig. 3a). Surprisingly, the respiratory dysbiosis was sustained at least 19-24 days after discharge (i.e., 42-58 days after symptom onset) in three children (CV01, CV02 and CV09).

In contrast, the gut microbiome alternation varied greatly among these COVID-19 children. Improvement or restoration was observed in three children (CV01, CV02 and CV05), but a worsening trend of unstable bacterial genera occurred in another three children (CV03, CV04 and CV09) (Fig. 3a). For example, the community type of CV09 improved from COVID-GUT-II to COVID-GUT-I on day 7 after symptom onset, but deteriorated to COVID-GUT-III on day 37. For CV03, whose microbiome got worse from a gut community type COVID-GUT-II on day 19 to a respiratory community type COVID-TN-III on day 27, and returned to COVID-GUT-II on day 43. The shift from a slightly dysbiosis gut community type to a severely dysbiosis respiratory community type implies microbial translocations from respiratory tract to gut. The restoration or worsening of the gut microbiome showed no association with clinical recovery (discharge from the hospital) or the presence or absence of SARS-CoV-2 RNA in the gut (Fig.3a).

Our data clearly demonstrate a progressively worsening of microbiome in both the respiratory tract and gut of children during the course of COVID-19. The worsening was predominantly driven by *Pseudomonas* species *P.veronii* (Fig. 3b and Supplementary Fig. 2), which was the most prevalent *Pseudomonas* species identified, and had a relative abundance of over 20% in most COVID-19 children. Genus *Streptococcus* (mainly *S.mitis*) also contributed to the worsening of the microbiome[22]. On the other hand, the presence of probiotic *Bifidobacterium* and the most important butyrate-

139 producing bacteria *Faecalibacterium* were inversely correlated with the existence of *Pseudomonas*
140 (Fig. 3b and Supplementary Fig. 2), despite these beneficial bacteria presented at a very low relative
141 abundance and often decreased in late disease stage.
142
143 **Bacteria–bacteria co-occurrence networks**
144 The co-occurrence network analysis revealed significant microbial cross-talk among different
145 body sites of children with COVID-19 (Fig. 4). There were three main co-occurrence networks
146 identified. Positive co-occurrence relationships were observed within and between bacteria from the
147 respiratory tract and the gut (FDR-adjusted $P<0.001$, Pearson correlation $r > 0.4$), indicating the
148 presence of frequent bacterial cross-talk between different body sites. Similar to our observation in
149 adults, the co-occurrence networks were relatively separated by different diversity-levels of
150 community types, but not by body sites. For example, bacteria from the community type COVID-
151 TN-III are closely associated with those from COVID-TN-II and COVID-GUT-II (Fig. 4). In this
152 network, *Pseudomonas* was positively correlated with some environmental bacteria. In another two
153 networks, probiotic (e.g. *Bifidobacterium* and *Faecalibacterium*) were mainly correlated with
154 commensals and community types H-MIX, COVID-GUT-I, COVID-TN-I and COVID-TN-II (Fig.
155 4). Therefore, the community types are more representative of microbiome status.

Discussion

SARS-CoV-2 infection causes damage to multiple organs either through direct infection, or indirectly disrupt host homeostasis, including perturbation of gut and respiratory microbiota in adults. Here, we report the first longitudinal investigation of microbiome with sampling from multiple anatomical sites of children with COVID-19, and present evidence that children have distinct differences compared to adults (Xu, unpublished observations), with respect to the dynamic changes of microbiota during the course of disease. The study of children is a significant feature because early-life microbiome plays important roles in the development of host immunity, metabolism, and neural systems, affecting profoundly health status in later life[7]. The microbiome attains a relatively stable adult-like structure at the age 3 after a highly dynamic initial developmental (months 3-14) phase, a transitional (months 15-30) phase, and finally a stable phase (months 31-46)[16]. The development of infants' microbiomes is more easily influenced by various internal (genetic) and external factors (e.g. birth mode, feeding type, siblings, antibiotics, and infection)[7,9], and maternal gut strains provide the largest contribution to the microbiome composition[15]. Early-life microbiome disruption caused by antibiotics and malnutrition is associated with increased risk of health problems later in childhood and even adulthood, such as developmental retardation, allergic diseases, obesity, diabetes and immune dysfunction[3-5,23,24].

SARS-CoV-2 infection impaired the respiratory and gut microbiota in both adults and children, but the respiratory and gut microbiome of children and adults faced diverging fates (Supplementary Fig. 3). In some mild adult cases, the respiratory and gut microbiomes showed a synchronous restoration from early dysbiosis towards later near-normal structure within a short period (6-17 days), substantially earlier than their clinical recovery (Xu et al. unpublished observation). In children,

178 however, the dynamic changes of the microbiome were divergent between respiratory tract and gut,
179 and the microbiome appeared to be progressively worsening, especially in the respiratory tract for a
180 long period (25-52 days), substantially later than their clinical recovery (12-37 days) (Supplementary
181 Fig. 3). In this cohort, six children were older than 3 years of age, and should have relatively stable
182 adult-like microbiome. The dynamic characteristics of the microbiome during COVID-19 implied
183 that children's microbiome is still particularly vulnerable and less resilient than that of the adults even
184 after attaining a stable phase[7,9,16]. Importantly, the persistent worsening of the microbiomes caused
185 by COVID-19 might impart potential short-term and long-term health problems during childhood and
186 adulthood.

187 We and other have reported that altered respiratory microbiome with reduced bacterial diversity
188 increased the susceptibility of children to acute respiratory tract infections (ARTIs)[6,8,25-27]. The
189 impaired microbiome in children with COVID-19 is characterized by *Pseudomonas*-dominated
190 community types that favor the colonization and growth of pathogenic and environmental bacteria,
191 and a reduction of some beneficial commensals (Fig. 4). Probiotic (e.g. *Bifidobacterium*) and
192 butyrate-producing bacteria (e.g. *Faecalibacterium*) that have anti-inflammatory ability were
193 extensively depleted from the gut and respiratory microbiomes of the children especially at late stage
194 of COVID-19 (Fig. 3b)[28,29]. Low abundance or lack of butyrate-producing bacteria might tolerate
195 low-level inflammation induced by SARS-CoV-2, rendering children more vulnerable to ARTIs and
196 diarrheal diseases[8,9,30]. In particular, the enrichment of genera *Moraxella* and *Streptococcus* in these
197 COVID-19 children might predispose them to an increased risk of recurrent ARTIs[6].

198 To the best of our knowledge, this is the first report on the complex dynamics of the gut and
199 respiratory microbiota in children with COVID-19. Disturbed development of both gut and

respiratory microbiomes, and prolonged respiratory dysbiosis caused by SARS-CoV-2 infection imply possible short-term and long-term complications after they have recovered from COVID-19, and predispose afflicted children to an increased health risk in later life. Although the long-term outcomes of COVID-19 on children need to be further studied with more extended follow-up and larger cohort, our data suggest that early implementation of various intervention strategies to modulate the microbiome development may provide clinical benefit to children in the post COVID-19 era.

Online content

Any methods, additional references, source data, extended data, supplementary information, acknowledgements, details of author contributions and competing interests, and statements of data and number availability are available.

1 Zhu, N. *et al.* A Novel Coronavirus from Patients with Pneumonia in China, 2019. *New Engl J Med* **382**, 727-733 (2020).

2 Zhou, P. *et al.* A pneumonia outbreak associated with a new coronavirus of probable bat origin. *Nature* **579**, 270-273 (2020).

3 Guan, W. *et al.* Clinical Characteristics of Coronavirus Disease 2019 in China. *New Engl J Med* **382**, 1708-1720 (2020).

4 Wu, Z. Y. & McGoogan, J. M. Characteristics of and Important Lessons From the Coronavirus Disease 2019 (COVID-19) Outbreak in China Summary of a Report of 72 314 Cases From the Chinese Center for Disease Control and Prevention. *Jama-J Am Med Assoc* **323**, 1239-1242 (2020).

5 Onder, G., Rezza, G. & Brusaferro, S. Case-Fatality Rate and Characteristics of Patients Dying in Relation to COVID-19 in Italy. *Jama-J Am Med Assoc* **323**, 1775-1776 (2020).

6 Teo, S. M. *et al.* The Infant Nasopharyngeal Microbiome Impacts Severity of Lower Respiratory Infection and Risk of Asthma Development. *Cell Host Microbe* **17**, 704-715 (2015).

7 Derrien, M., Alvarez, A. S. & de Vos, W. M. The Gut Microbiota in the First Decade of Life. *Trends Microbiol* **27**, 997-1010 (2019).

8 Dubourg, G., Edouard, S. & Raoult, D. Relationship between nasopharyngeal microbiota and patient's susceptibility to viral infection. *Expert Rev Anti-Infe* **17**, 437-447 (2019).

9 Man, W. H., Piters, W. A. A. D. & Bogaert, D. The microbiota of the respiratory tract: gatekeeper to respiratory health. *Nat Rev Microbiol* **15**, 259-270 (2017).

10 Blanton, L. V. *et al.* Gut bacteria that prevent growth impairments transmitted by microbiota from malnourished children. *Science* **351**, 10.1126/science.aad3311 aad3311 (2016).

11 Gehrig, J. L. *et al.* Effects of microbiota-directed foods in gnotobiotic animals and undernourished children. *Science* **365**, eaau4732 (2019).

12 Cox, L. M. *et al.* Altering the Intestinal Microbiota during a Critical Developmental Window Has Lasting Metabolic Consequences. *Cell* **158**, 705-721 (2014).

13 Gu, S. *et al.* Alterations of the Gut Microbiota in Patients with COVID-19 or H1N1 Influenza. *Clin Infect Dis*, ciaa709 (2020).

14 Zuo, T. *et al.* Alterations in Gut Microbiota of Patients With COVID-19 During Time of Hospitalization. *Gastroenterology*, ciaa709 (2020).

15 Ferretti, P. *et al.* Mother-to-Infant Microbial Transmission from Different Body Sites Shapes the Developing Infant Gut Microbiome. *Cell Host Microbe* **24**, 133-145.e135 (2018).

16 Stewart, C. J. *et al.* Temporal development of the gut microbiome in early childhood from the TEDDY study. *Nature* **562**, 583-588 (2018).

17 Ding, T. & Schloss, P. D. Dynamics and associations of microbial community types across the human body. *Nature* **509**, 357-360 (2014).

18 Chen, Y. J. *et al.* Parasutterella, in association with irritable bowel syndrome and intestinal chronic inflammation. *J Gastroen Hepatol* **33**, 1844-1852 (2018).

19 Cheuk, W., Woo, P. C. Y., Yuen, K. Y., Yu, P. H. & Chan, J. K. C. Intestinal inflammatory pseudotumour with regional lymph node involvement: identification of a new bacterium as the aetiological agent. *J Pathol* **192**, 289-292 (2000).

20 Spilker, T., Vandamme, P. & LiPuma, J. J. Identification and distribution of Achromobacter species in cystic fibrosis. *J Cyst Fibros* **12**, 298-301 (2013).

21 Jones, A. M. *et al.* Burkholderia cenocepacia and Burkholderia multivorans: influence on survival in cystic fibrosis. *Thorax* **59**, 948-951 (2004).

22 Mitchell, J. Streptococcus mitis: walking the line between commensalism and pathogenesis. *Mol Oral Microbiol* **26**, 89-98 (2011).

23 Livanos, A. E. *et al.* Antibiotic-mediated gut microbiome perturbation accelerates development of type 1 diabetes in mice. *Nat Microbiol* **1**, 16140 (2016).

24 Grier, A. *et al.* Neonatal gut and respiratory microbiota: coordinated development through time and space. *Microbiome* **6**, 193 (2018).

25 Man, W. H. *et al.* Bacterial and viral respiratory tract microbiota and host characteristics in children with lower respiratory tract infections: a matched case-control study. *Lancet Resp Med* **7**, 417-426 (2019).

26 Langevin, S. *et al.* Early nasopharyngeal microbial signature associated with severe influenza in children: a retrospective pilot study. *J. Gen. Virol.* **98**, 2425-2437 (2017).

27 Piters, W. A. A. D. *et al.* Nasopharyngeal Microbiota, Host Transcriptome, and Disease Severity in Children with Respiratory Syncytial Virus Infection. *Am J Resp Crit Care* **194**, 1104-1115 (2016).

28 Riviere, A., Selak, M., Lantin, D., Leroy, F. & De Vuyst, L. Bifidobacteria and Butyrate-Producing Colon Bacteria: Importance and Strategies for Their Stimulation in the Human Gut. *Frontiers in Microbiology* **7**, 979 (2016).

29 Lopez-Siles, M., Duncan, S. H., Garcia-Gil, L. J. & Martinez-Medina, M. Faecalibacterium prausnitzii: from microbiology to diagnostics and prognostics. *Isme J* **11**, 841-852 (2017).

30 Li, Y. P. *et al.* Altered respiratory virome and serum cytokine profile associated with recurrent respiratory tract infections in children. *Nat Commun* **10**, 2288 (2019).

Figure legends

Fig. 1. Dirichlet multinomial mixtures (DMM) clustering analyses of 16S rRNA data separate COVID-19 children into groups with distinctive features (*N* = 128). a. Eight distinct clusters were identified based on lowest Laplace approximation for control and patient samples from gut or nasal and throat cavities. Heat map showing the relative abundance of 40 most dominant bacterial genera per DMM cluster. The stars represent unclassified genera. H-GUT indicates abnormal gut microbial community structure of healthy children. H-MIX represents normal microbial community structure of a mixture of fecal, nasal and throat samples of healthy individuals. COVID-GUT I-III enriched in fecal samples of COVID-19 children; COVID-TN I-III enriched in both nasal and throat samples of COVID-19 children. b. Nonmetric multidimensional scaling (NMDS) visualization of DMM clusters using Bray-Curtis distance of bacterial genera. Significant separation of microbial community structures was implicated by the ANOSIM statistic R closer to 1 with < 0.05 P value. The stress value lower than 0.2 provides a good representation in reduced dimensions. **c**. Box plots showing the alpha diversity (richness and evenness) per each DMM cluster. Wilcoxon test was used to compare difference of H-MIX cluster and others under three significance levels of * P < 0.05, **P<0.01, and ***P<0.001.

Fig. 2. Identification (a) and relative abundance distribution (b) of indicator genera of eight DMM clusters. Indicators of eight microbial community types (DMM clusters) were identified from top 40 genus contributing to DMM clustering in Fig.1a (See Supplementary Methods). Twenty-one indicator genera are shared by two or more community types with similar diversity levels (e.g. II-III, or I-H-MIX). Significance levels of indicators are as follows: * P <0.05, ** P <0.01, and *** P <

298 0.001.

299

300 **Fig. 3. Dynamic change of both DMM clusters (a) and six key taxa (b) in three body sites of**
301 **COVID-19 children.** Age (months) of each COVID-19 child was shown in brackets. The community
302 type levels were divergent between respiratory tract and gut (e.g. on days 11, 15 and 23 in CV04, and
303 days 16 and 42 in CV09). The respiratory microbiome appeared to be progressively worsening in
304 seven children (CV01-CV04 and CV07-CV09) for 25-42 days after symptom onset. The worsening
305 of the gut microbiome appeared in four children (CV03, CV04, CV07 and CV09), and sustained for
306 25-52 days. **b**, key taxa of DMM clusters were shown in eight COVID-19 children with at least two
307 time points of sampling. Linked to Supplementary Fig.2.

308

309 **Fig. 4. Co-occurrence network of gut, nasal and throat microbiotas in the progression of**
310 **COVID-19 children.** Positively correlated microbial pairs with both Pearson correlation r values
311 higher than 0.4 and FDR-adjusted P values lower than 0.001 were shown.

Method

Study population

Nine children were diagnosed as COVID-19 patients by Children's Hospital of Fudan University according to the National Guidelines for Diagnosis and Treatment of COVID-19. A total of 103 samples, including 31 nasal swabs, 28 throat swabs and 44 feces, were collected from these patients (Supplementary Fig. S1). Twenty-five samples from 14 age-matched healthy children were used as controls. The respiratory samples were collected using flexible, sterile, dry swabs, which can reach the posterior nasopharynx and oropharynx easily (approximately 2 inches). About 2 ml spontaneous, unstimulated fecal specimen (300 mg/tube) was collected into a sterile cryogenic vial (Corning, NY, USA), divided into aliquots and stored at –80 °C until use. The sampling was performed by the professionals at the hospital.

The study was approved by Children's Hospital of Fudan University (2020-27). Informed consents were obtained from involved patients or their guardians.

Confirmation of COVID-19 children

The clinical and epidemiological characteristics, and SARS-CoV-2 RNA shedding patterns of these patients were previously reported[31,32]. All nine COVID-19 children had mild symptoms. The virus RNA was extracted from all samples using a Mag-Bind RNA Extraction Kit (MACCURA, Sichuan, China) according to the manufacturer's instructions. The *ORFlab* and *N* genes of SARS-CoV-2 was detected using a Novel Coronavirus (2019-nCoV) RNA detection Kit (PCR-Fluorescence Probing) (DAAN gene, Guangzhou, China) according to the manufacturer's instructions.

334 **16S rRNA gene sequencing**

335 All samples including nasal swabs, throat swabs and stool samples were subjected to the DNA
336 extraction using a QIAamp DNA Microbiome Kit (QIAGEN, Düsseldorf, Germany). A novel triple-
337 index amplicon sequencing strategy was used for 16S rRNA gene sequencing[33]. In brief, a set of
338 universal bacterial primers was used to amplify the V4 hypervariable region (515-806 nt) of the 16S
339 rRNA gene. Two rounds of PCR amplifications were performed [34]. A reaction mixture containing 8
340 μL Nuclease-free water, 0.5 μL KOD-Plus-Neo (TOYOBO, Osaka Boseki, Japan), 2.5 μL of 1 μM
341 PCR1 forward primer, 2.5 μL of 1 μM PCR1 reverse primer, and 5 μL DNA template was prepared
342 for the first round of the PCR (PCR1) amplification. PCR1 products were purified using Monarch
343 DNA Gel Extraction Kit (New England Biolabs, Ipswich, MA, USA), and quantified by a Qubit®
344 4.0 Fluorometer (Invitrogen, Carlsbad, CA, USA). Purified PCR1 products were pooled with equal
345 amounts, and then subjected to the secondary round of PCR (PCR2) amplification. The PCR2 mix
346 contains 21 μL Nuclease-free water, 1 μL KOD-Plus-Neo (TOYOBO, Osaka Boseki, Japan), 5 μL of
347 1 μM PCR2 forward primer, 5 μL of 1 μM PCR2 reverse primer, and 5 μL pooled PCR1 products.
348 The PCR2 products were purified using the same Gel Extraction Kit and qualified using the Qubit®
349 4.0 Fluorometer. The specific products were further qualified using Agilent 2100 Bioanalyzer
350 (Agilent, Santa Clara, CA, USA). The PCR2 products with equal moles of specific products were
351 pooled and mixed them with AMPure XP beads (Beckman Coulter, Pasadena, CA, USA) in a ratio of
352 0.8:1. After purification, the amplicons were paired-end sequenced (2x250) using Illumina-P250
353 sequencer.

354

355 **Bioinformatic analysis of 16S rRNA gene sequence data**

Using USEARCH11 software[35] and FASTX-Toolkit[36], sequenced reads were merged, de-multiplexed and filtered. After trimming barcode, adapter and primer sequences using USEARCH11, 14,702, 896 sequences were retained with an average of 100019 sequences per sample. Based on the Qiime2 platform[37], the Deblur[38] was used to cluster sequence data into sub-OTUs (operational taxonomic units), better than traditional OTU picking usually according to 97% sequence similarity threshold which may miss subtle and real biological sequence variation[39]. In particular, we used the Deblur to perform quality control, dereplicate, chimeras remove on with default settings except for truncating sequence length to 250bp. A sub-OTU (sOTU) count table, equivalent to OTU table, was generated (2187 sOTUs). The taxonomic classification of sOTU representative sequences was assigned by using the RDP Naive Bayesian Classifier algorithm[40] based on the Ribosomal Database project (RDP) 16S rRNA training set (v16) database[41]. Finally, the sOTU table were subsampled at an even depth of 3600 sequences per sample to eliminate the bias led by different sequencing depths among samples. The sOTU coverage of 87% was sufficient to capture microbial diversity.

Identification and characteristics of microbial community types

Based on the bacterial genus abundance, we used the Dirichlet multinomial mixtures (DMM)[42] algorithm introduced by mothur[43] v1.44.1 to identify microbial community types because the DMM algorithm could efficiently cluster samples based on microbial composition, whose sensitivity, reliability and accuracy were widely confirmed in many microbiome studies[16,44,45]. Based on the lowest Laplace approximation index, the appropriate microbial community type numbers (DMM clusters) were determined. Conjugated with the Analysis of Similarities (ANOSIM), the reliability of DMM clustering was further validated and then visualized by the Non-metric multidimensional

scaling (NMDS) based on the Bray-Curtis distance under bacterial genus level. "The ANOSIM statistic "R" compares the mean of ranked dissimilarities between groups to the mean of ranked dissimilarities within groups. An R value close to "1.0" suggests dissimilarity between groups while an R value close to "0" suggests an even distribution of high and low ranks within and between groups[46]. ANOSIM p values lower than 0.05 suggest the higher similarity within sites. Richness (Observed sOTUs) and Pielou's or Species evenness for each community type were calculated for estimating the difference of alpha diversity. Those analyses described above were performed using R package "vegan" v2.5-6. Using R package 'Pheatmap', the dynamic change of microbial community types and compositions were visualized. Alpha diversity difference between groups were measured using the Wilcoxon Rank Sum Test in R.

Identification of indicator taxa contributing to microbial community typing

To get the reliable indicator genus for community typing, we performed the Indicator Species Analysis using the indicspecies package (ver.1.7.8) [47] in R platform with top 40 genus contributing to DMM clustering that accounted for 71% cumulative difference. Dynamic changes of indicator genera corresponding to each community type were showed in all COVID-19 children using the pheatmap package in R.

Co-occurrence network analysis of microbiomes among gut, nasal, and throat of COVID-19 children

Based on microbial genus abundances of gut, nasal, and throat samples collected from 8 COVID-19 children, we calculated the Pearson Correlation Coefficient (Pearson's r) among bacterial genera of

three body sites. The Pearson's r higher than 0.4 or lower than -0.4 with *P* values that were below 0.05 after the FDR adjustment were considered significant correlation. Co-occurrence network of significantly correlated bacterial genus pairs was visualized using Cytoscape v3.8.0[48].

Data availability

The raw data of 16S rRNA gene sequences are available at NCBI Sequence Read Archive (SRA) (https://www.ncbi.nlm.nih.gov/sra/) at BioProject ID PRJNA642019.

31 Cai, J. *et al.* A Case Series of children with 2019 novel coronavirus infection: clinical and epidemiological features. *Clin Infect Dis*, ciaa198 (2020).

32 Liu, P. *et al.* Dynamic surveillance of SARS-CoV-2 shedding and neutralizing antibody in children with COVID-19. *Emerg Microbes Infect* **9**, 1254-1258 (2020).

33 D'Amore, R. *et al.* A comprehensive benchmarking study of protocols and sequencing platforms for 16S rRNA community profiling. *Bmc Genomics* **17**, 55 (2016).

34 de Muinck, E. J., Trosvik, P., Gilfillan, G. D., Hov, J. R. & Sundaram, A. Y. M. A novel ultra high-throughput 16S rRNA gene amplicon sequencing library preparation method for the Illumina HiSeq platform. *Microbiome* **5**, 68 (2017).

35 Edgar, R. C. UPARSE: highly accurate OTU sequences from microbial amplicon reads. *Nature Methods* **10**, 996-998 (2013).

36 Hannon, G. J. FASTX-Toolkit. *http://hannonlab.cshl.edu/fastx_toolkit* (2010).

37 Caporaso, J. G. *et al.* QIIME allows analysis of high-throughput community sequencing data. *Nature Methods* **7**, 335-336 (2010).

38 Amir, A. Deblur rapidly resolves single-nucleotide community sequence patterns. *mSystems.* **2** (2017).

39 Knight, R. *et al.* Best practices for analysing microbiomes. *Nature Reviews Microbiology* **16**, 410-422 (2018).

40 Wang, Q., Garrity, G. M., Tiedje, J. M. & Cole, J. R. Naïve Bayesian Classifier for Rapid Assignment of rRNA Sequences into the New Bacterial Taxonomy. *Applied and Environmental Microbiology* **73**, 5261 (2007).

41 Cole, J. R. *et al.* Ribosomal Database Project: data and tools for high throughput rRNA analysis. *Nucleic Acids Research* **42**, D633-D642 (2013).

42 Holmes, I., Harris, K. & Quince, C. Dirichlet Multinomial Mixtures: Generative Models for Microbial Metagenomics. *PLoS ONE* **7**, e30126 (2012).

43 Schloss, P. D. *et al.* Introducing mothur: open-source, platform-independent, community-supported software for describing and comparing microbial communities. *Appl Environ Microbiol* **75**, 7537-7541 (2009).

44 Ding, T. & Schloss, P. D. Dynamics and associations of microbial community types across the human body. *Nature* **509**, 357-360 (2014).

45 Fujimura, K. E. *et al.* Neonatal gut microbiota associates with childhood multisensitized atopy and T cell

differentiation. *Nature Medicine* **22**, 1187-1191 (2016).

46 Clarke, K. R. Non-parametric multivariate analyses of changes in community structure. *Australian Journal of Ecology* **18**, 117-143 (1993).

47 De Cáceres, M., Legendre, P. & Moretti, M. Improving indicator species analysis by combining groups of sites. Oikos 119, 1674-1684 (2010).

48 Otasek, D., Morris, J. H., Boucas, J., Pico, A. R. & Demchak, B. Cytoscape Automation: empowering workflow-based network analysis. Genome Biol 20, 185 (2019).

Author contributions C.Z. conceived the study idea. C.Z., Z.Z. and J.X designed and supervised the study. P.L., M.Z. and J.X collected clinical samples and data. R.X., P.L. and Y.M. performed the experiments. T.Z. and Q.W. processed and analyzed the raw sequencing data. R.X., P.L., J.X. and M.Z. analyzed the clinical data. C.Z., Z.Z. and X.J. interpreted the data. Z.Z. and R.X. generated the figures. C.Z., Z.Z., R.X., and T.Z. wrote the first draft of the manuscript. X.J. contributed to critical revision. All authors contributed to the final manuscript.

Acknowledgements We thank Mr. Kai Liu and Mrs. Xiuming Wu at Institut Pasteur of Shanghai, Chinese Academy of Sciences for their technical support. This work was supported by the grants from the National Key Research and Development Program of China (2017ZX10103009-002 and 2018YFC2000500), the Second Tibetan Plateau Scientific Expedition and Research (STEP) program (2019QZKK0503), the Key Research Program of the Chinese Academy of Sciences (FZDSW-219), the Chinese National Natural Science Foundation (31970571) and grants specific for Coronavirus Disease 2019 from the Children's Hospital of Fudan University (Grant No. EKXGZX006).

Competing interests The authors declare no competing interests.

Additional information

Supplementary Table S1. Fecal, nasal, and throat microbial abundances (phyla and genera). The stars represent unclassified genera.

Supplementary Fig. S1. COIVD-19 patient admission and discharge times as well as the detection of SARS-CoV-2. DAY 1 was the day of symptom onset.

Supplementary Fig. S2. Dynamic change of 26 indicator genera in three body sites of nine COVID-19 children. Linked to Fig.2a and Fig.3b. The stars represent unclassified genera.

Supplementary Fig. S3. Distinct gut and respiratory microbiome mechanisms associated with the progress of COVID-19 in adults and children. The dynamic mechanism of the microbiome in adults was interpreted from our recent observation based on the longitudinal throat and anal swabs from 35 adults with COVID-19 (Xu et al. unpublished data). Similar community types from I to III/IV indicate a progressive dysbiosis of the microbiome. In mild adults with COVID-19, a synchronous shift of community type from early dysbiosis towards late incomplete restoration was found in both respiratory and gut microbiomes within a short time. In children, however, the changes of the community types were divergent between the respiratory tract and gut, possibly implying that the "airway-gut axis" is still not established during the childhood. Moreover, children's respiratory microbiome appeared to be progressively worsening for a long period despite a fast clinical recovery.

Fig.1

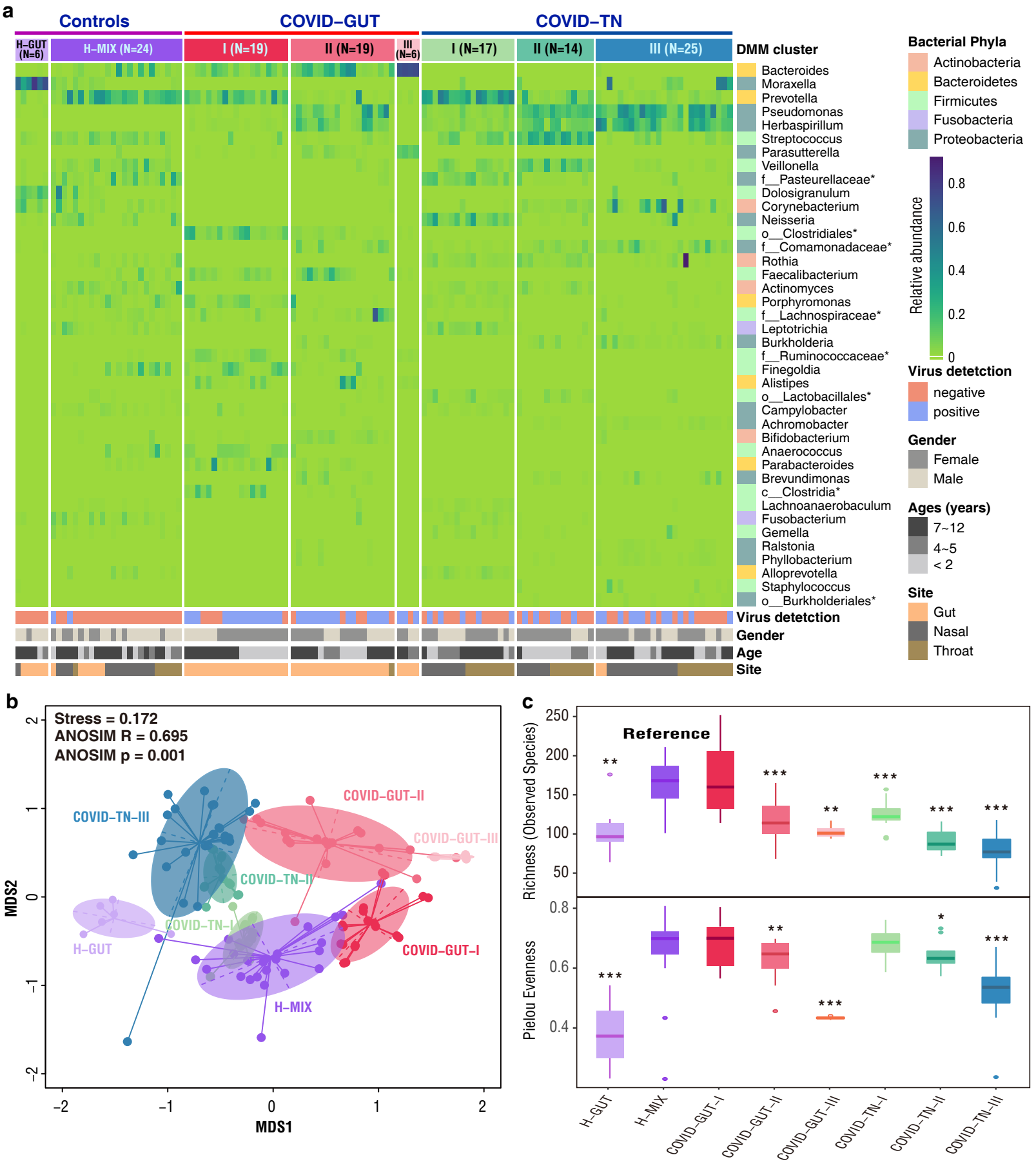
a
Controls
COVID–GUT
COVID–TN
H–GUT (N=6)
H–MIX (N=24)
I (N=19)
II (N=19)
III (N=6)
I (N=17)
II (N=14)
III (N=25)
DMM cluster
Bacteroides
Moraxella
Prevotella
Pseudomonas
Herbaspirillum
Streptococcus
Parasutterella
Veillonella
f__Pasteurellaceae*
Dolosigranulum
Corynebacterium
Neisseria
o__Clostridiales*
f__Comamonadaceae*
Rothia
Faecalibacterium
Actinomyces
Porphyromonas
f__Lachnospiraceae*
Leptotrichia
Burkholderia
f__Ruminococcaceae*
Finegoldia
Alistipes
o__Lactobacillales*
Campylobacter
Achromobacter
Bifidobacterium
Anaerococcus
Parabacteroides
Brevundimonas
c__Clostridia*
Lachnoanaerobaculum
Fusobacterium
Gemella
Ralstonia
Phyllobacterium
Alloprevotella
Staphylococcus
o__Burkholderiales*
Virus detetction
Gender
Age
Site
Bacterial Phyla
Actinobacteria
Bacteroidetes
Firmicutes
Fusobacteria
Proteobacteria
Relative abundance
0.8
0.6
0.4
0.2
0
Virus detetction
negative
positive
Gender
Female
Male
Ages (years)
7~12
4~5
< 2
Site
Gut
Nasal
Throat
b
Stress = 0.172
ANOSIM R = 0.695
ANOSIM p = 0.001
COVID–TN–III
COVID–GUT–II
COVID–GUT–III
COVID–TN–II
COVID–TN–I
H–GUT
COVID–GUT–I
H–MIX
MDS1
MDS2
c
Reference
Richness (Observed Species)
Pielou Evenness
H–GUT
H–MIX
COVID–GUT–I
COVID–GUT–II
COVID–GUT–III
COVID–TN–I
COVID–TN–II
COVID–TN–III

Fig. 2

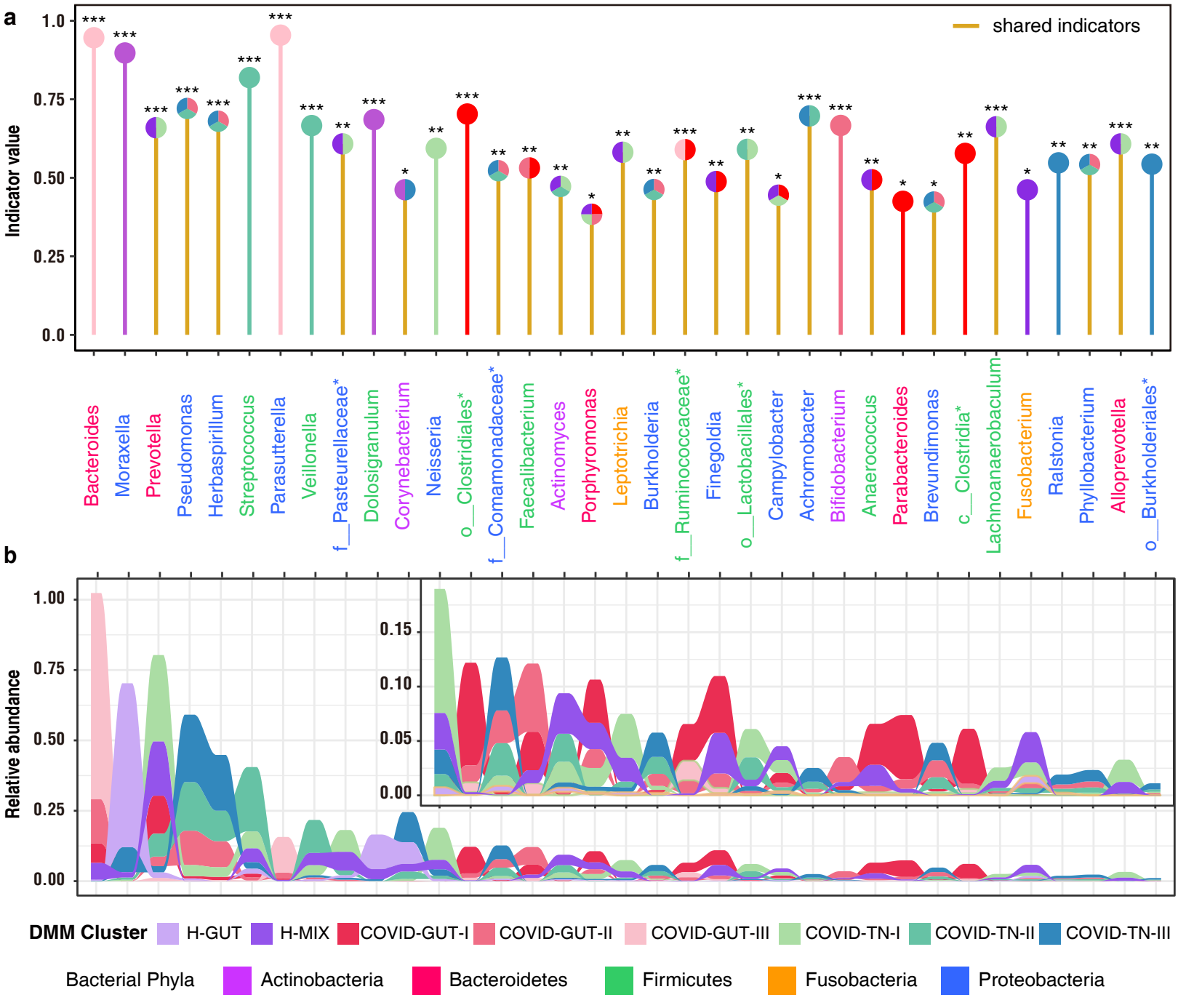
a
shared indicators
Indicator value
1.0
0.75
0.50
0.25
0.0
Bacteroides
Moraxella
Prevotella
Pseudomonas
Herbaspirillum
Streptococcus
Parasutterella
Veillonella
f__Pasteurellaceae*
Dolosigranulum
Corynebacterium
Neisseria
o__Clostridiales*
f__Comamonadaceae*
Faecalibacterium
Actinomyces
Porphyromonas
Leptotrichia
Burkholderia
f__Ruminococcaceae*
Finegoldia
o__Lactobacillales*
Campylobacter
Achromobacter
Bifidobacterium
Anaerococcus
Parabacteroides
Brevundimonas
c__Clostridia*
Lachnoanaerobaculum
Fusobacterium
Ralstonia
Phyllobacterium
Alloprevotella
o__Burkholderiales*
b
Relative abundance
1.00
0.75
0.50
0.25
0.00
0.15
0.10
0.05
0.00
DMM Cluster
H-GUT
H-MIX
COVID-GUT-I
COVID-GUT-II
COVID-GUT-III
COVID-TN-I
COVID-TN-II
COVID-TN-III
Bacterial Phyla
Actinobacteria
Bacteroidetes
Firmicutes
Fusobacteria
Proteobacteria

Fig. 3

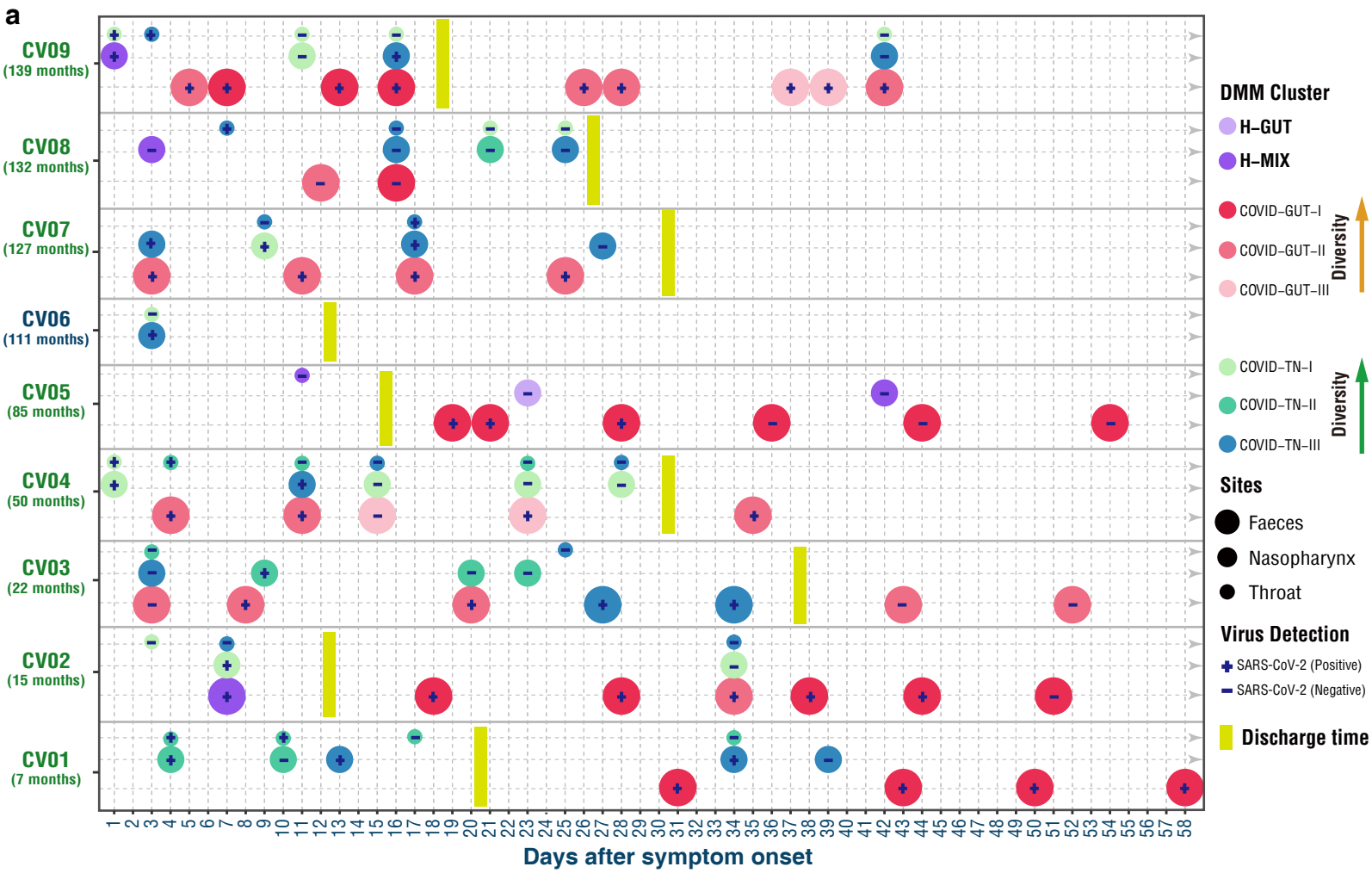
a
CV09 (139 months)
CV08 (132 months)
CV07 (127 months)
CV06 (111 months)
CV05 (85 months)
CV04 (50 months)
CV03 (22 months)
CV02 (15 months)
CV01 (7 months)
Days after symptom onset
DMM Cluster
H-GUT
H-MIX
COVID-GUT-I
COVID-GUT-II
COVID-GUT-III
Diversity
COVID-TN-I
COVID-TN-II
COVID-TN-III
Diversity
Sites
Faeces
Nasopharynx
Throat
Virus Detection
SARS-CoV-2 (Positive)
SARS-CoV-2 (Negative)
Discharge time

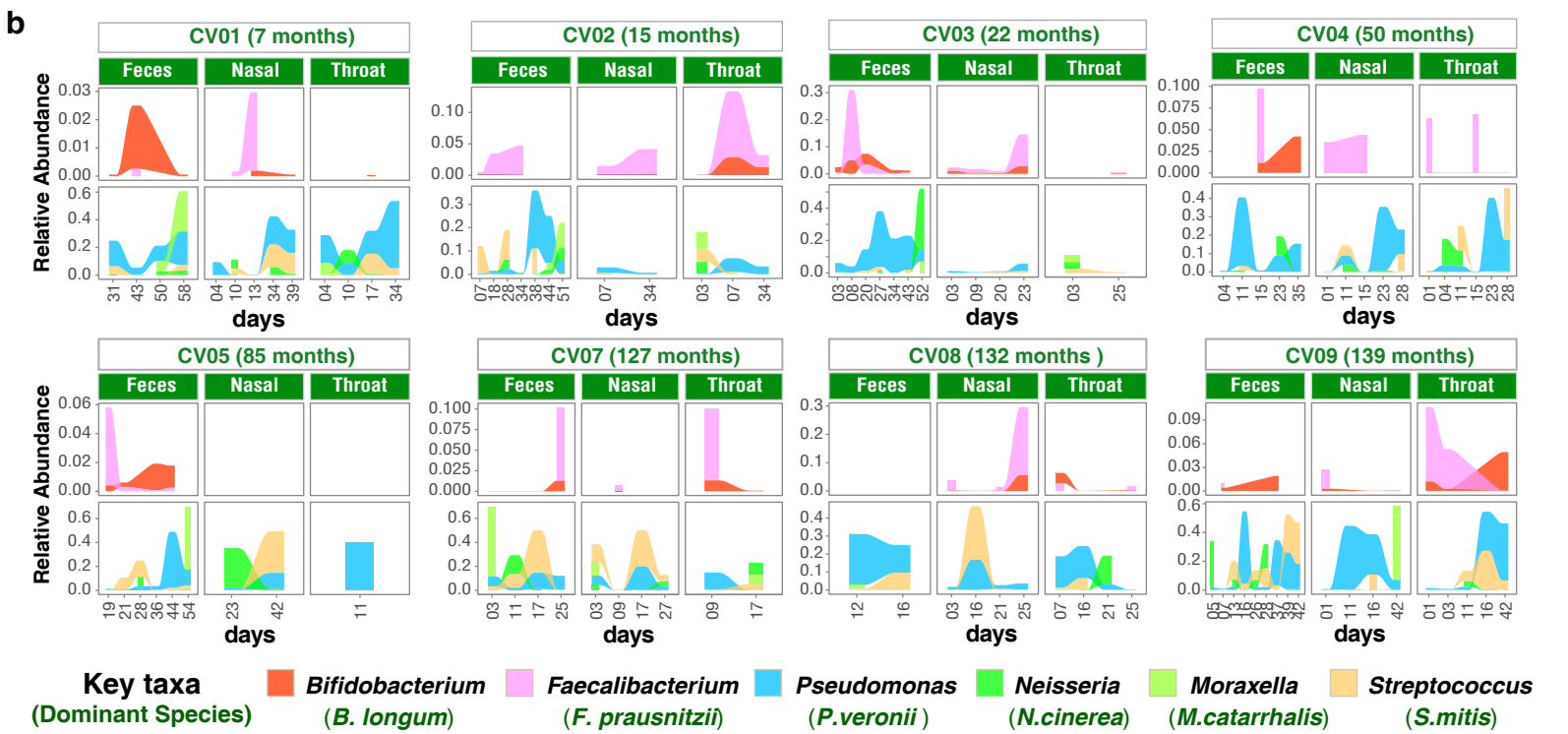
b
CV01 (7 months)
CV02 (15 months)
CV03 (22 months)
CV04 (50 months)
CV05 (85 months)
CV07 (127 months)
CV08 (132 months)
CV09 (139 months)
Feces
Nasal
Throat
Relative Abundance
days
Key taxa
(Dominant Species)
Bifidobacterium (B. longum)
Faecalibacterium (F. prausnitzii)
Pseudomonas (P.veronii)
Neisseria (N.cinerea)
Moraxella (M.catarrhalis)
Streptococcus (S.mitis)

Fig.4

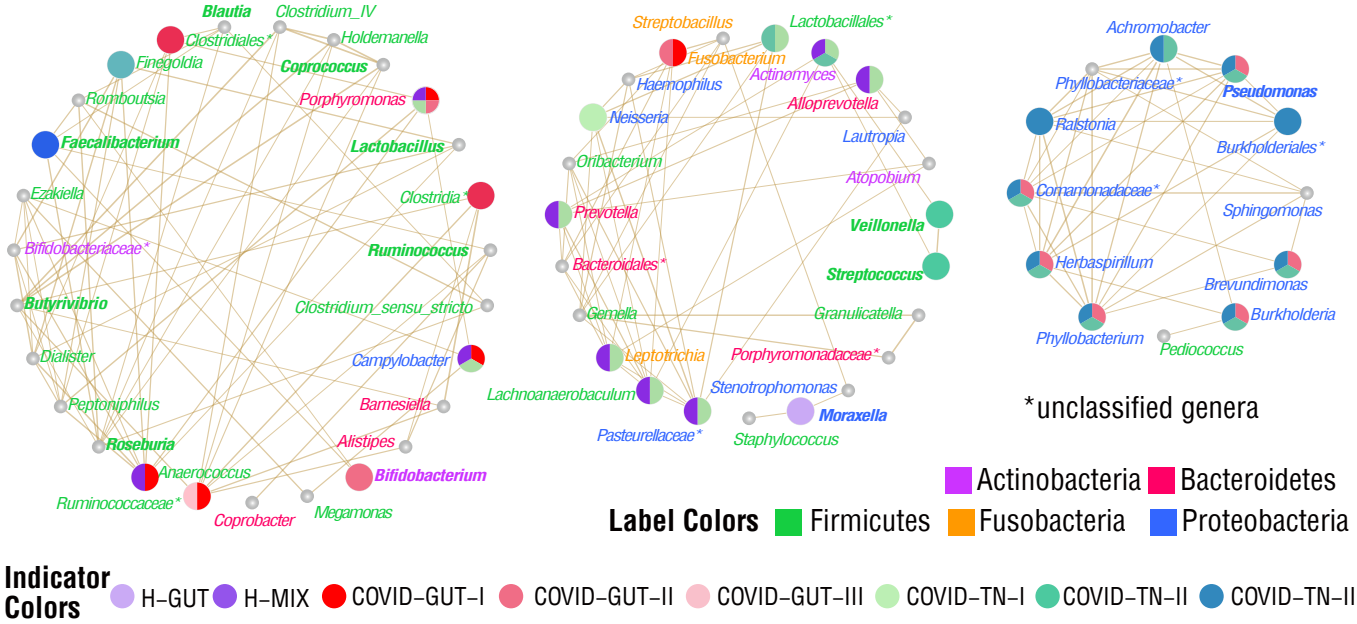
Blautia
Clostridium_IV
Clostridiales*
Holdemanella
Finegoldia
Coprococcus
Romboutsia
Porphyromonas
Faecalibacterium
Lactobacillus
Ezakiella
Clostridia*
Bifidobacteriaceae*
Ruminococcus
Butyrivibrio
Clostridium_sensu_stricto
Dialister
Campylobacter
Peptoniphilus
Barnesiella
Roseburia
Alistipes
Anaerococcus
Bifidobacterium
Ruminococcaceae*
Coprobacter
Megamonas
Streptobacillus
Lactobacillales*
Fusobacterium
Actinomyces
Haemophilus
Alloprevotella
Neisseria
Lautropia
Oribacterium
Atopobium
Prevotella
Veillonella
Bacteroidales*
Streptococcus
Gemella
Granulicatella
Leptotrichia
Porphyromonadaceae*
Lachnoanaerobaculum
Stenotrophomonas
Moraxella
Pasteurellaceae*
Staphylococcus
Achromobacter
Phyllobacteriaceae*
Pseudomonas
Ralstonia
Burkholderiales*
Comamonadaceae*
Sphingomonas
Herbaspirillum
Brevundimonas
Burkholderia
Phyllobacterium
Pediococcus
*unclassified genera
Actinobacteria
Bacteroidetes
Label Colors
Firmicutes
Fusobacteria
Proteobacteria
Indicator Colors
H-GUT
H-MIX
COVID-GUT-I
COVID-GUT-II
COVID-GUT-III
COVID-TN-I
COVID-TN-II
COVID-TN-III